Chinese Journal of Chemical Engineering 53 (2023) 251–259

Contents lists available at ScienceDirect

Chinese Journal of Chemical Engineering

journal homepage: www.elsevier.com/locate/CJChE

Full Length Article

Silicalite-1 zeolite encapsulated Fe nanocatalyst for Fenton-like degradation of methylene blue

Hongwei Guo [1], Linyuan Chen [2], Xueying Zhang [2], Huanhao Chen [1,*], Yan Shao [2,*]

[1] State Key Laboratory of Materials-Oriented Chemical Engineering, College of Chemical Engineering, Nanjing Tech University, Nanjing 211816, China
[2] School of Environmental Science and Engineering, Nanjing Tech University, Nanjing 211816, China

ARTICLE INFO

Article history:
Received 10 October 2021
Received in revised form 25 February 2022
Accepted 1 March 2022
Available online 23 March 2022

Keywords:
Zeolite
Encapsulation
Fe nanocatalyst
Degradation
Methylene blue

ABSTRACT

Encapsulation of Fe nanoparticles in zeolite is a promising way to significantly improve the catalytic activity and stability of Fe-based catalysts during the degradation process of organic pollutants. Herein, Fe nanocatalysts were encapsulated into silicalite-1 (S-1) zeolite by using a ligand-protected method (with dicyandiamide (DCD) as a organic ligand) under direct hydrothermal synthesis condition. High-resolution transmission electron microscopy (HRTEM) results confirmed the high dispersion of Fe nanocatalysts which were successfully encapsulated within the voids among the primary particles of the S-1 zeolite. The developed S-1 zeolite encapsulated Fe nanocatalyst (Fe@S-1) exhibited significantly improved catalytic activity and reusability in the catalytic degradation process of methylene blue (MB). Specifically, the developed $Fe_{0.021}$@S-1 catalyst showed high catalytic degradation activity, giving a high MB degradation efficiency of 100% in 30 min, outperformed the conventional impregnated catalyst (Fe/S-1). Moreover, the Fe@S-1 catalyst afforded an outstanding stability, showing only *ca.* 7.9% activity loss after five cycling tests, while the Fe/S-1 catalyst presented a significantly activity loss of 50.9% after only three cycles. Notably, the encapsulation strategy enabled a relatively lower Fe loading in the Fe@S-1 catalyst in comparison with that of the Fe/S-1 catalyst, *i.e.,* 0.35% *vs.* 0.81% (mass). Radical scavenging experiments along with electron spin resonance (ESR) measurements confirmed that the major role of ·OH in the MB degradation process. Specifically, Fe@S-1 catalyst with high molar ratio of $[Fe(DCD)]Cl_3$ is beneficial to form Fe complexes/nanoclusters in the voids (which has large pore size of 1–2 nm) among the primary particles of the zeolite, and thus improving the diffusion and accessibility of reactants to Fe active sites, and thus exhibiting a relatively higher degradation efficiency. This work demonstrates that zeolite-encapsulated Fe nanocatalysts present potential applications in the advanced oxidation of wastewater treatment.

1. Introduction

Fenton-like degradation is one of an advanced oxidation process (AOP) for catalytic elimination of organic pollutants such as dyes (*e.g.*, methylene blue, MB) in wastewater [1–5]. In recent years, application of Fenton-like degradation for organic wastewater treatment is mostly based on heterogeneous catalysts [5,6]. Many metal-based catalysts have been developed for Fenton-like degradation system in order to efficiently activate H_2O_2 to produce ·OH, showing good activity for degrading organic compounds [7,8]. Among them, Fe-based catalysts have been widely developed because of their high activity, extensive supply as well as low cost [5,9]. However, heterogeneous Fe-based catalysts still present some drawbacks such as poor accessibility and stability of the active Fe sites [6]. To overcome these limitations, porous materials (*e.g.*, zeolite [6,10,11], ordered mesoporous carbon [12]) were used as support for Fe oxide particles in order to reduce the metal particle size, and therefore develop robust catalysts for Fenton-like degradation system. However, for practical application of Fenton-like degradation, it is still challenging to develop a robust heterogeneous Fenton catalyst which has improved metal dispersion and stability.

Zeolites have attracted interest due to their unique structure and properties (such as well-defined microporous channels and excellent hydrothermal stability), being an ideal support to stabilize metal nanoparticles [6,13–17]. However, zeolite supported

* Corresponding authors.
E-mail addresses: h.chen@njtech.edu.cn (H. Chen), y.shao@njtech.edu.cn (Y. Shao).

https://doi.org/10.1016/j.cjche.2022.03.010
1004-9541/

metal catalysts prepared by simple impregnation methods normally generate relatively larger metal particles with poor dispersion located in zeolite channels and/or on the external surface of zeolite, and thus presenting low activity and stability [14]. One alternative strategy of manipulating the dispersion and particle size of metal sites in zeolite-based catalysts is to *in situ* encapsulate metal sites during hydrothermal synthesis of zeolite, which could efficiently control the size and location of metal nanoparticles, and therefore improving the stability of metal active sites [18]. Dai *et al.* [6] employed an "impregnation-dissolution-recrystallization" method to encapsulate highly dispersed Fe-Cu bimetallic oxide nanoparticles within silicalite-1 (S-1) zeolite, and the resulting catalyst exhibited high dispersion of Fe-Cu oxide with average particle size of ~3.7 nm, showing high catalytic activity and low leaching of metal oxide for Fenton-like degradation of phenol. However, this strategy requires a multi-step procedure, as the tetrapropylammonium hydroxide (TPAOH) hydrothermal treatment needed to facilitate the dissolution and recrystallization of zeolite supported catalysts is carried out in a separate step. Recently, many efforts have been devoted to developing simple yet efficient strategies for the encapsulation of metal sites within zeolites [13–20]. Cho *et al.* [18] reported a cationic polymer-assisted method to successfully encapsulate Pt nanocatalysts inside MFI zeolites. Pt@HZSM-5 catalyst exhibited high encapsulation degree of Pt nanoparticles in zeolite (exceeding 90%), giving high selectivity for aldol condensation and hydrogenation, displaying combined yield of 87% for hydrogenated C_8 products. Recently, Yu and co-workers prepared sub-nanometer Pd clusters within nanosized S-1 zeolite by using a ligand-stabilized method (employing $[Pd(en)_2]Cl_2$ (en = ethylenediamine) as precursor) [13]. The developed catalysts present an excellent activity toward the complete formic acid decomposition to efficiently generated H_2 (696 L $H_2 \cdot h^{-1}$ $(g \cdot Pd)^{-1}$).

Herein, we employed a ligand-stabilized method to confine Fe nanoparticles within S-1 zeolite (*i.e.*, Fe@S-1) by using dicyandiamide ($C_2H_4N_4$, DCD) as an organic ligand. The developed catalysts present outstanding activity and reusability for the Fenton-like degradation of MB.

2. Experimental

2.1. Chemicals

Tetraethyl orthosilicate (TEOS, 98%), Ferric chloride ($FeCl_3 \cdot 5H_2O$), tetrapropylammonium hydroxide aqueous solution (TPAOH, 25 %(mass)), hydrogen peroxide (H_2O_2, 30 %(mass)) were supplied from Sinopharm Chemical Reagent Co., Ltd. Dicyandiamide (DCD, $(N_2H)_2CN_2$), tert-butyl alcohol (TBA), benzoquinone (BQ) were supplied by Shanghai Lingfeng Chemical Reagent Co., Ltd. Methylene blue (MB) was purchased from Wuxi Yasheng Chemical Co., Ltd.

2.2. Synthesis of the Fe@S-1 catalysts

Fig. 1 shows the strategy for developing S-1 zeolite encapsulated Fe catalyst. $[Fe(DCD)]Cl_3$ as the precursor was prepared firstly. Specifically, 1.26 g of dicyandiamide was dissolved into 10 ml deionized (DI) water, followed by adding 0.15 g of $FeCl_3 \cdot 5H_2O$, and the solution was continuously stirred at room temperature (RT). The synthesis gel for Fe@S-1 catalyst was prepared according to different molar composition: 1.0TEOS: 0.4TPAOH: $35H_2O$: $x[Fe(DCD)]Cl_3$ (x = 0.002, 0.005, 0.014, 0.021, 0.029, respectively) [17]. Typically, 6.5 g of TPAOH solution was firstly added in 7.5 g of DI water, followed by the slow addition of 4.16 g TEOS, and then the solution was stirred for 6 h until fully hydrolyze the TEOS. After that, the prepared $[Fe(DCD)]Cl_3$ solution was added slowly and the solution was stirred for additional 0.5 h. Subsequently, the resulting gel was transferred into a 50 ml Teflon-lined stainless-steel autoclave, and the hydrothermal synthesis was carried out in an oven at 170 °C for 3 days. After the hydrothermal synthesis, the as-prepared samples were washed with DI water for several times, and then dried at 100 °C overnight, and finally calcined at 550 °C for 6 h in air. The prepared catalysts were named based on the adding amount of Fe, *i.e.,* Fe_x@S-1 (x = 0.002, 0.005, 0.014, 0.021, 0.029, respectively). In addition, reference catalyst with a nominal Fe loading of 1.0 %(mass) was prepared by conventional incipient wetness impregnation method, *i.e.,* Fe/S-1.

2.3. Characterization of materials

The actual metal content in as-prepared catalysts were measured using Inductively Coupled Plasma Atomic Emission Spectroscopy (ICP-OES 5000, Focused Photonics Inc.). The crystallinity of the samples was characterized by powder X-ray diffraction (XRD) employed a Smartlab TM 9kw (Rigaku) advance diffractometer with Cu K_α radiation (λ = 0.15418 nm). The prepared catalysts were measured using a high-resolution transmission electron microscopy (HRTEM, FEI Tecnai G2 F20) and corresponding energy dispersive X-ray spectroscopy (EDS). Raman spectra were measured by using a high-resolution confocal Raman spectrometer with a 50 × LWD objective lens. Electron spin resonance (ESR) spectra were obtained on a Bruker EMX-10/12 to detect the reactive oxygen species (ROS). Specifically, the 5, 5-dimethyl-1-pyrroline N-oxide (DMPO) were employed as spin-trap reagent. In addition, radical scavenging experiments were conducted by the addition of a corresponding ROS scavengers during the catalytic degradation process of MB.

2.4. Catalytic degradation performance tests

MB was used to evaluate the degradation efficiency of Fe@S-1 catalysts. Specifically, for each experiment, 50 mg catalyst was added into MB solution (100 ml, 10 $mg \cdot L^{-1}$) under 60 °C without stirring (the initial pH value was 2). Prior to the addition of H_2O_2, the suspension was continuously stirred for about 20 min to reach the adsorption and desorption equilibrium between MB and catalyst, followed by adding 4 ml H_2O_2. At given time intervals, sample (2 ml) was collected and filtered off by using a needle filter (0.22 μm pore size). The supernatant was analyzed by recording variations at 665 nm using a UV-725 UV–visible spectrophotometer (Shanghai Youke Instrument Co., Ltd). To test the reusability of Fe@S-1 catalyst, after each experiment, catalysts were collected from suspension, followed by centrifuging and washing with DI water several times. After that, the recovered catalysts were tested again according to same procedure. The degradation efficiency of MB can be calculated as:

$$\text{MB degradation} = \frac{C_0 - C_t}{C_0} \times 100\ \% \quad (1)$$

where C_0 ($mg \cdot L^{-1}$) and C_t ($mg \cdot L^{-1}$) are the MB concentrations at time zero and t, respectively.

3. Results and Discussion

3.1. Characterization of catalysts

As shown in Fig. 1, the nitrogen atoms on nitrile bond ($N^{(1)}$ and $N^{(2)}$) and imine bond ($N^{(3)}$ and $N^{(4)}$) in DCD molecule are suitable electron donors to readily interact with Fe due to their lone pair electrons and high charge density. Therefore, Fe^{3+} could strongly coordinate with DCD molecule to form $[Fe(DCD)]Cl_3$ complex

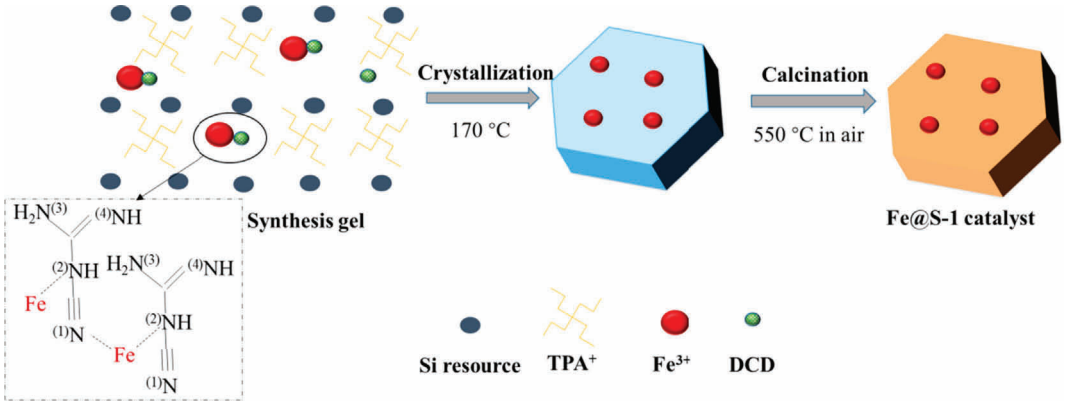

Fig. 1. Schematic of the preparation strategy of silicalite-1 zeolite encapsulated Fe catalyst.

avoiding Fe precipitation in solution. The complex as a precursor could enable the encapsulation of Fe complexes/nanoclusters in zeolite under one-pot hydrothermal synthesis condition. The actual Fe loading in as-prepared Fe@S-1 catalyst along with Fe/S-1 (as reference catalyst) was determined by using ICP-OES, as listed in Table S1 in Supporting Information (SI).

Fig. 2 shows the Raman spectra of Fe@S-1 catalyst (exemplified by $Fe_{0.005}$@S-1) before and after calcination. As seen in Fig. 2, the band located at *ca.* 368 cm^{-1} corresponds to the characteristic of the MFI-type zeolite structure [21]. For the Fe@S-1 catalyst before calcination (Fig. 2(a)), the Raman bands located at *ca.* 1036, 1102, and 2975 cm^{-1} could be attributed to the DCD molecule's C—N═C symmetric stretching and bending, N—C—N asymmetric stretching, as well as NH_2 stretching, respectively [22]. Significantly, the characteristic band of N—C≡N bending (located at *ca.* 659 cm^{-1}) shows weak intensity, which should be due to the interaction between Fe species and N—C≡N [22]. However, for the Fe@S-1 catalyst after calcination (Fig. 2(b)), all characteristic peaks related to DCD molecule disappeared due to the burning-out of DCD molecule under high temperature condition, while Fe species were successfully encapsulated in S-1 zeolite. Specifically, after calcination, the intensity of Raman band located at *ca.* 504 cm^{-1} (this should be due to isolated Fe—O—Si bonds positioned at extra-framework [23,24]) decreased significantly, further illustrating Fe species encapsulated in S-1 zeolite. Additionally, as shown in Fig. 2, the bands at *ca.* 295 and 420 cm^{-1} (which could be assigned to the Fe_2O_3 structure [21]) are hardly observed, implying that most of Fe species were well encapsulated in S-1 zeolite.

Fig. 3 shows the powder XRD patterns of as-prepared Fe@S-1 catalysts. As shown in Fig. 2, XRD measurements revealed that all Fe-containing catalysts presented the MFI topological structure with several characteristic diffraction peaks (*i.e.* 2θ = 7.9°, 8.8°, 23.1°, 23.9°, and 24.4°), respectively [25], implying that the lattice distortion was negligible after encapsulating Fe species inside S-1 zeolite [17]. It is worth noting that the characteristic diffraction peaks related to Fe species were not detected, indicating the absence of large Fe particles in the as-prepared Fe@S-1 catalysts.

HRTEM analysis of the Fe@S-1 and Fe/S-1 catalysts were performed to provide the detailed information regarding the location and dispersion of Fe species in the S-1 zeolite, as shown in Figs. 4 and 5. Comparative HRTEM images of the Fe@S-1 catalysts with different molar ratio of $[Fe(DCD)]Cl_3$ in the synthesis gel (*i.e.*, 0.005, 0.014, 0.021, 0.029, respectively) shows the typical coffin-like morphology of S-1 zeolite (Fig. 4(a), (d), (g), and (j)). Specifically, by increasing the molar ratio of $[Fe(DCD)]Cl_3$, the particle size of prepared S-1 zeolites gradually increased from ~ 290 nm to ~ 500 nm. For $Fe_{0.005}$@S-1 and $Fe_{0.014}$@S-1 catalysts (Fig. 4(b), (c), (e) and (f)), TEM analysis showed the transparent S-1 crystals with crystal lattice of *ca.* 0.58 nm, on which Fe species are hardly identified, indicating that Fe could be atomically incorporated into the MFI-type zeolite framework. Similarly, Yu *et al.* [17] have proved that single Rh atoms can be encapsulated within 5-membered rings of S-1 zeolite framework by using [Rh(NH_2CH_2-

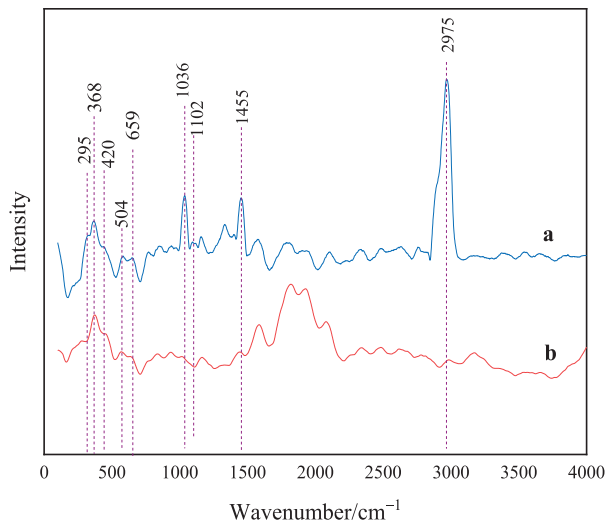

Fig. 2. Raman spectra of $Fe_{0.005}$@S-1 catalyst before and after calcination: (a) before, and (b) after.

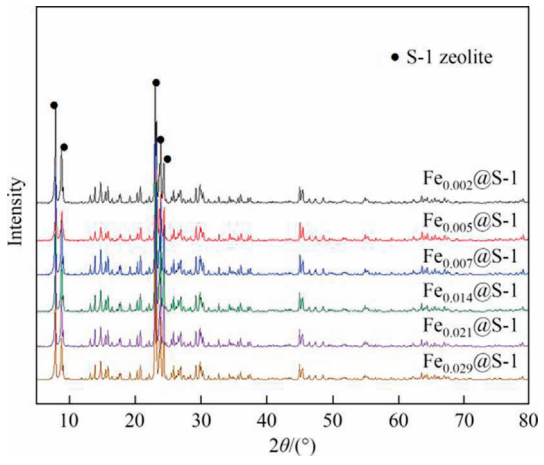

Fig. 3. XRD patterns of as-prepared Fe@S-1 catalysts.

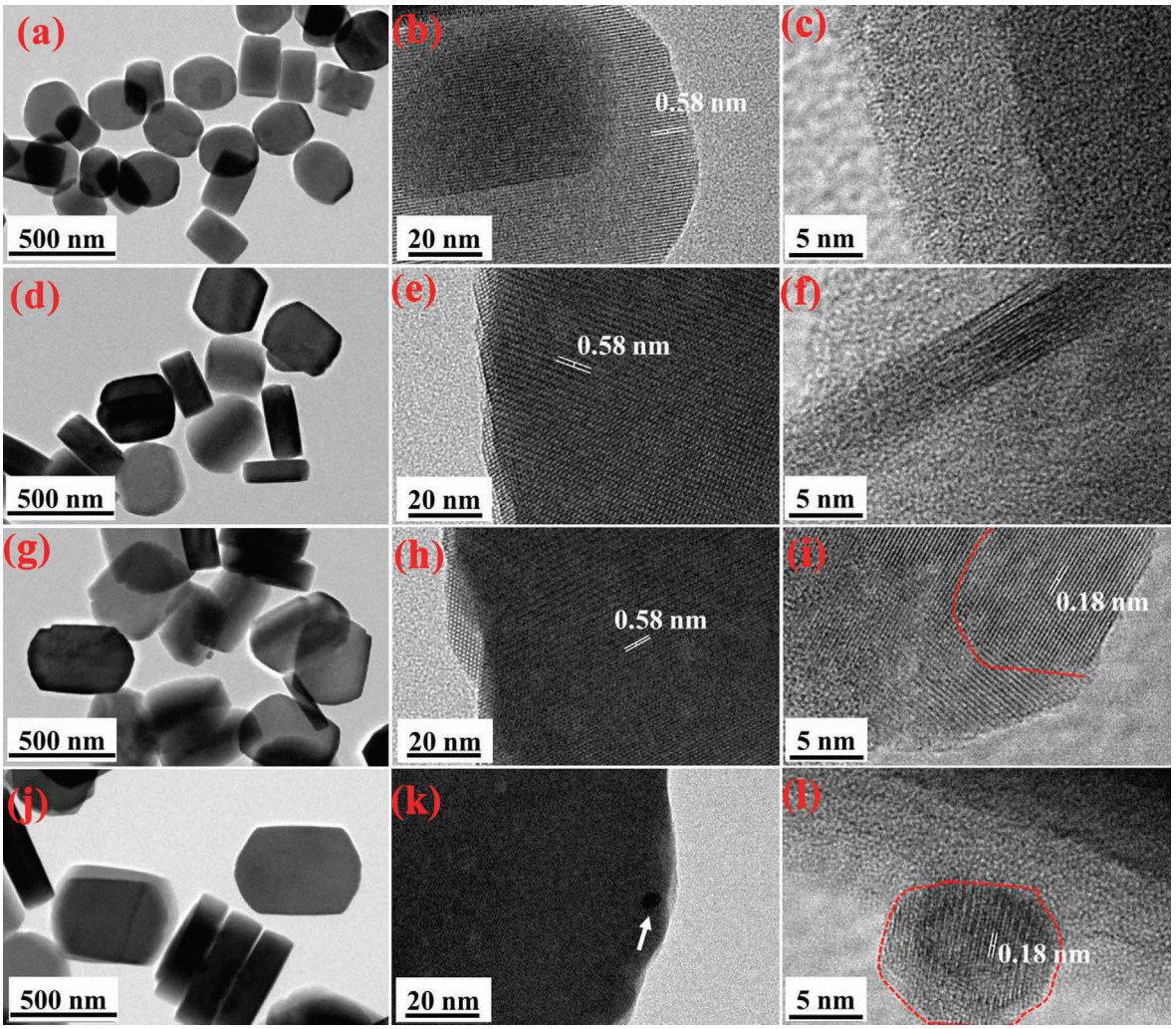

Fig. 4. High-resolution transmission electron microscopy images of Fe@S-1 catalysts with different Fe contents: (a-c) 0.005, (d-f) 0.014, (g-i) 0.021, (j-l) 0.029.

$CH_2NH_2)_3]Cl_3$ complex as a precursor. However, when the molar ratio of $[Fe(DCD)]Cl_3$ increased to 0.021 ($Fe_{0.021}$@S-1), TEM analysis shows non-transparent S-1 crystal (Fig. 4(h)) and Fe species with crystal lattice of *ca.* 0.18 nm in S-1 zeolite (Fig. 4(i)), suggesting that Fe complexes/nanoclusters with larger particle size are likely to be formed in the voids among the primary zeolite particles. By increasing the molar ratio up to 0.029 ($Fe_{0.029}$@S-1), Fe nanoparticles are formed both in the voids among the primary zeolite particles (referred by white arrow in Fig. 4(k)) and on the external surface (with particle size of ~ 10 nm, referred by red circle in Fig. 4(l)) of S-1 zeolite. For Fe/S-1 catalyst, as shown in Fig. 5(a)–(c), Fe particles with relatively larger particle size (~9.8 nm) were formed on the external surface of zeolite.

EDS mapping analysis of Fe@S-1 catalyst (Fig. 6) shows the dispersion of different elements (*e.g.*, Fe, referred by red spots). As shown in Fig. 6a and b, Fe element in the $Fe_{0.005}$@S-1 and $Fe_{0.014}$@S-1 catalysts was less visible, implying that Fe species in the encapsulated zeolite coating were relatively lower, being in line with the ICP-OES results shown in Table S1 and Fig. S1 in Supplementary Material. However, by increasing the $[Fe(DCD)]Cl_3$ amount in the synthesis gel, Fe element become visible in EDS mapping images of the $Fe_{0.021}$@S-1 and $Fe_{0.029}$@S-1 catalysts (Fig. 6(c) and (d)), suggesting the formation of redundant Fe species on the external surface of S-1 zeolite. Additionally, as shown in Fig. S2, the encapsulated Fe@S-1 catalysts have a much lighter red colour compared to bulk impregnated Fe/S-1 catalyst, while the colour gradually turns red by increasing the molar ratio of Fe in catalysts. These results further confirm the formation of redundant Fe species on the external surface of zeolite, which is in accordance with the HRTEM results.

3.2. Catalytic degradation performances of MB over the Fe@S-1 catalysts

We further utilize the MB degradation process to evaluate the activity trends of Fe@S-1 catalyst with H_2O_2 at a constant temperature of 60 °C (initial MB concentration of 10 mg·L^{-1}, initial solution pH = 2). As shown in Fig. 7(a), the blank experiment using the H_2O_2 showed the insignificant degradation efficiency of MB. However, the encapsulated $Fe_{0.005}$@S-1 catalyst exhibited a relatively faster MB degradation process compared to the impregnated Fe/S-1 catalyst with high Fe loading of 0.81% (mass) (Table S1), which is two-fold of that of the $Fe_{0.005}$@S-1 catalyst (0.35 %(mass)). By comparison, it proves that the encapsulation method gave a relatively low Fe loading (Table S1), but a relatively higher dispersion of Fe species than that of conventional impregnated catalyst (which is confirmed by the HRTEM results in Fig. 5), achieving improved catalytic activity and reusability (which will be discussed later). As shown in Fig. 7(b), by increasing the molar ratio of Fe in encapsulated catalysts up to 0.029, the Fe@S-1 catalysts

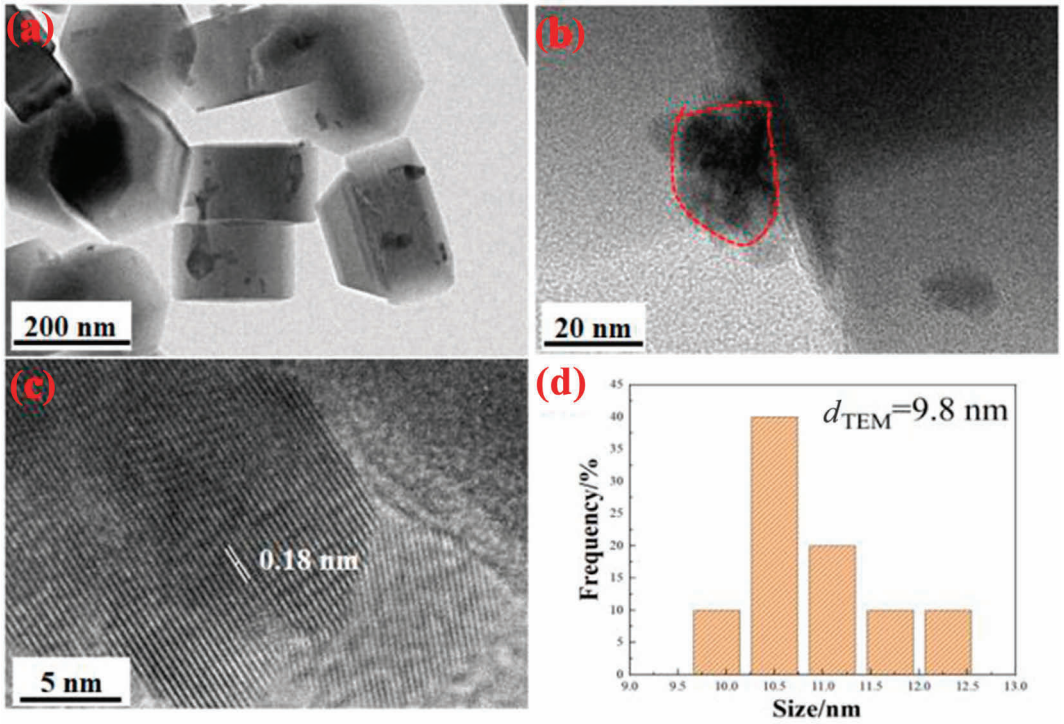

Fig. 5. High-resolution transmission electron microscopy images of reference catalyst (Fe/S-1): (a-c) HRTEM images with different resolution, (d) corresponding Fe particle size distribution of the Fe/S-1 catalyst.

(with molar ratio of Fe > 0.014) displayed the highest catalytic degradation rate, eliminating the organic compound in 10 min. Additionally, to clearly compare the degradation activities of the Fe@S-1 catalysts with different Fe contents, the catalytic degradation performance evaluation experiments were further performed using a higher initial MB concentration (100 $mg{\cdot}L^{-1}$). Clearly, as shown in Fig. 8, the catalytic degradation rate of the Fe@S-1 catalysts significantly increased by increasing of Fe molar ratio from 0.002 to 0.021, suggesting that the increased Fe loading in the encapsulated catalyst benefited the formation of Fe complexes/-nanocluster (which is confirmed by the HRTEM results in Fig. 4 (a)–(i)) and thus improved the catalytic activity. Specifically, according to TEM results (Fig. 4), when the molar ratio of [Fe (DCD)]Cl_3 in the synthesis gel is low (*e.g.* 0.005, 0.014), Fe could be atomically incorporated into the MFI-type silicalite-1 zeolite framework. The long and narrow pore channels (~0.55 nm) of S-1 zeolite could limit the diffusion of reactants (*i.e.* Methylene Blue, H_2O_2) and products (*i.e.* CO_2 and H_2O), and thus inhibiting the accessibility of reactants to Fe active sites. Consequently, these Fe@S-1 catalysts exhibited a relatively poor degradation efficiency. However, when increasing the molar ratio of [Fe(DCD)]Cl_3 up to 0.021, Fe complexes/nanoclusters with larger particle size are likely to be formed in the voids (which has larger pore size of 1–2 nm) among the primary particles of the zeolite, which will significantly promote the diffusion and accessibility of reactants to Fe active sites, and enabling a relatively higher degradation efficiency. Notably, when further increasing the molar ratio of Fe up to 0.029, the $Fe_{0.029}$@S-1 catalyst exhibited a relatively lower degradation rate compared with that of the $Fe_{0.021}$@S-1 catalyst. This might attribute to the formation of Fe nanoparticles with larger particle size (~10 nm) on the external surface of S-1 zeolite (Fig. 4(i)–(l)), which could block the pores of voids among the primary zeolite particles and inhibit the accessibility of reactants to Fe active sites with smaller particle size (encapsulated inside zeolite), and thus giving low MB degradation rate.

We further evaluated the catalytic stability of $Fe_{0.005}$@S-1 catalyst in the degradation of MB by five cycling tests, experiment results were shown in Fig. 9. Clearly, as shown in Fig. 9(a), there is a slight decline of degradation rate from 99.6% to 91.7%, showing *ca.* 7.9% activity loss after five cycles. However, impregnated Fe/S-1 catalyst exhibited a relatively poor reusability, *i.e.*, the degradation rate significantly decreased from 68.8% to 33.7% after three cycles. These results further demonstrate that the encapsulation of Fe species into S-1 zeolite could significantly improve the stability of Fe active sites, and thus preventing their leaching during the catalytic degradation process. Additionally, as shown in Fig. 9(b), the XRD results confirm that the S-1 zeolite structure of $Fe_{0.005}$@S-1 catalyst remained rather stable during the cycling MB degradation tests. Additionally, as shown in Table 1, the MB degradation performance of the developed Fe@S-1 catalyst was also compared with that of previously reported catalysts. The Fe@S-1 catalyst demonstrates slightly better catalytic degradation efficiency than the reported catalysts (*e.g.* graphene supported Fe_3O_4, Fe_3O_4/GO, *etc*), although that the Fe loading (*i.e.* 0.35 %(mass)) in Fe@S-1 catalyst is significant low.

3.3. Catalytic degradation mechanism of MB over the Fe@S-1 catalyst

To confirm the role of the main active species, the activity of $Fe_{0.005}$@S-1catalyst was further explored using different scavengers for the ·OH and $\cdot O_2^-$, such as *tert*-butyl alcohol (TBA) and p-benzoquinone (BQ) [4]. As shown in Fig. 10(a), in the presence of BQ, the degradation rate of MB was still up to *ca.* 80% in 60 min, which suggests that the $\cdot O_2^-$ could not be the main active species for the MB degradation. However, in the presence of TBA, the catalytic MB degradation rate significantly declined to *ca.* 50% in 60 min, indicating that the ·OH should be the major reactive species. ESR spin trap was also used to confirm the radicals generated by the Fe@S-1 catalyst during the MB degradation process, with DMPO as a radical trapper, and the results are shown in

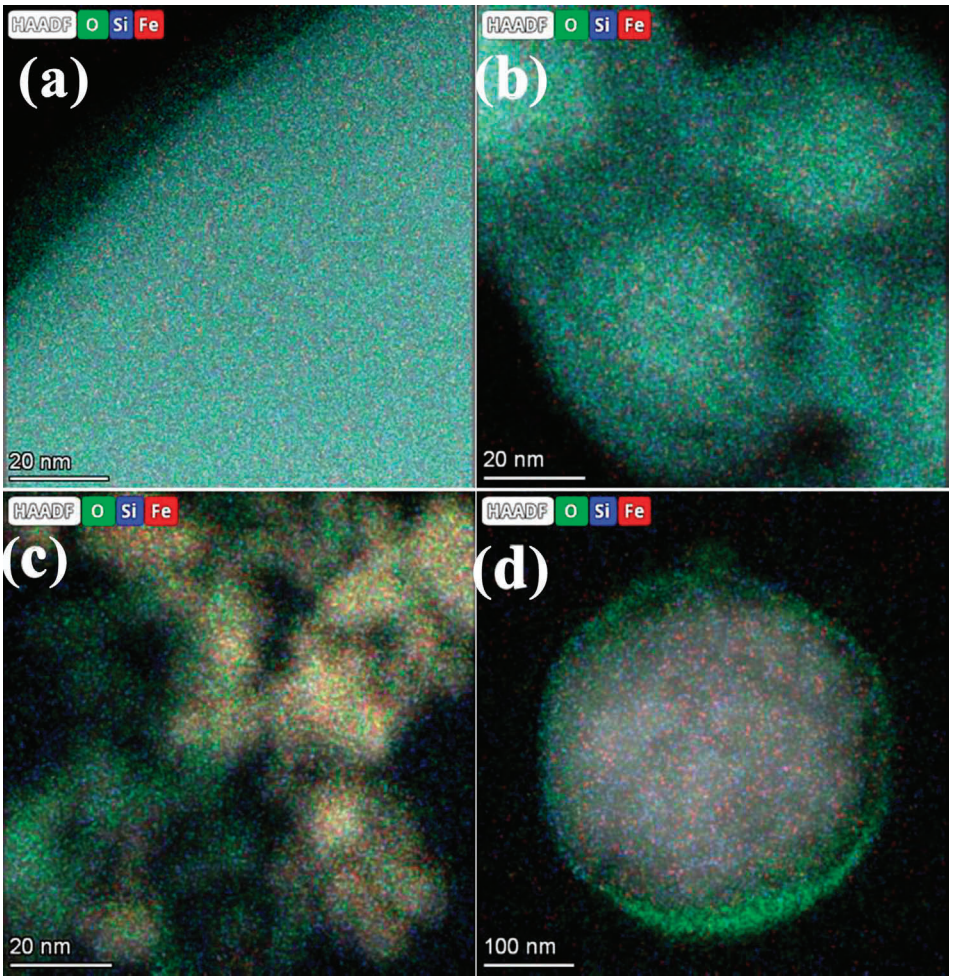

Fig. 6. EDS mapping analysis of Fe@S-1 catalysts with different Fe contents: (a) 0.005, (b) 0.014, (c) 0.021, (d) 0.029. (Red spots: the Fe element).

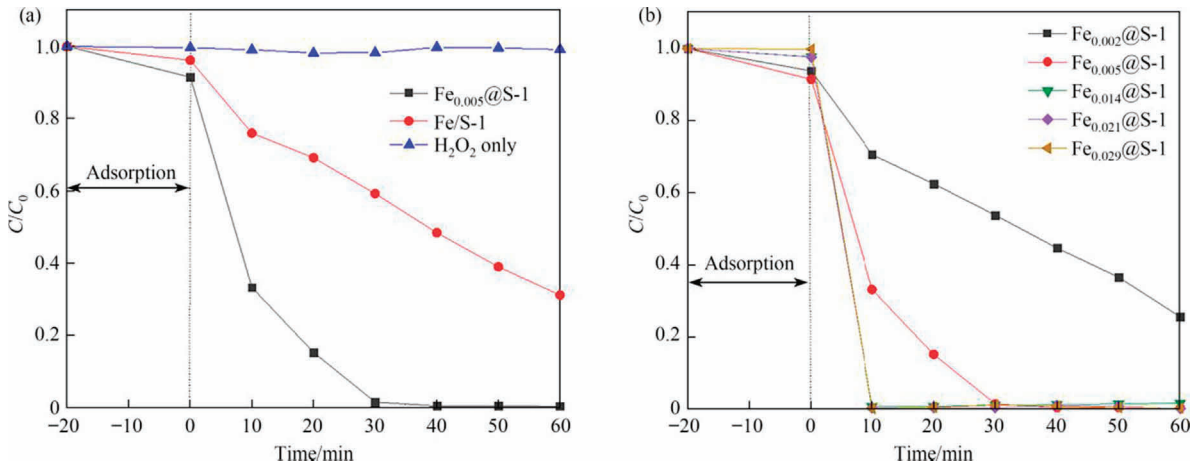

Fig. 7. Catalytic degradation performances of catalysts: (a) comparative performances of $Fe_{0.005}$@S-1 and Fe/S-1, and (b) performances of Fe@S-1 catalysts with different molar ratio of Fe. Reaction conditions: [MB] = 10 mg·L^{-1}, catalyst = 0.5 g·L^{-1}, [H_2O_2] = 4 mmol·L^{-1}, T = 60 °C, initial solution pH = 2. (Adsorption refers to the insignificant physical adsorption of MB on the Fe@S-1 catalyst).

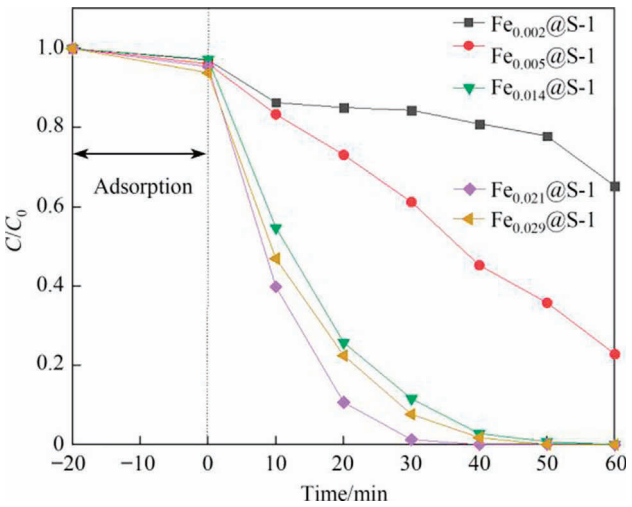

Fig. 8. Catalytic degradation performances of Fe@S-1 catalysts with different molar ratio of Fe. Reaction condition: [MB] = 100 mg·L^{-1}, catalyst = 0.5 g·L^{-1}, [H_2O_2] = 4-mmol·L^{-1}, T = 60 °C, initial solution pH = 2. (Adsorption refers to the insignificant physical adsorption of MB on the Fe@S-1 catalyst).

Fig. 10(b). Clearly, the ESR spin trap results demonstrated the DMPO−·OH peaks with strong intensities generated by the $Fe_{0.005}$@S-1catalyst, confirming the key role of ·OH during the MB degradation process. Additionally, the characteristic peaks of DMPO−·O_2^- with weak intensities were also detected.

Based on the above findings, the possible mechanism was proposed and shown in Fig. 11. Typically, during the catalytic degradation process, the MB and H_2O_2 molecules diffused in the voids (which has large pore size of 1–2 nm) among the primary particles of the zeolite and interacted with Fe(Ⅱ) species from Fe complexes/nanoclusters which were encapsulated in the Fe@S-1, following by the rapid formation of Fe(III) and ·OH (Eqs. (2) and (3)). Subsequently, the ·OH radicals will readily attack the MB molecules which already diffused into the voids, and thus producing small molecules, which were fully destroyed into CO_2 and H_2O. Meanwhile, the Fe(III) species will be also reduced by H_2O_2 to generate Fe(II) and ·O_2^- species (Eq. (4)), ensuring the recycling formation of Fe(II) species [26]. However, for the catalysts with low molar ratio of [Fe(DCD)]Cl_3, the diffusion and accessibility of reactants and products to Fe active sites could be significantly limited due to that most of Fe species were atomically incorporated into the zeolite framework, and thus exhibiting a relatively lower degradation efficiency.

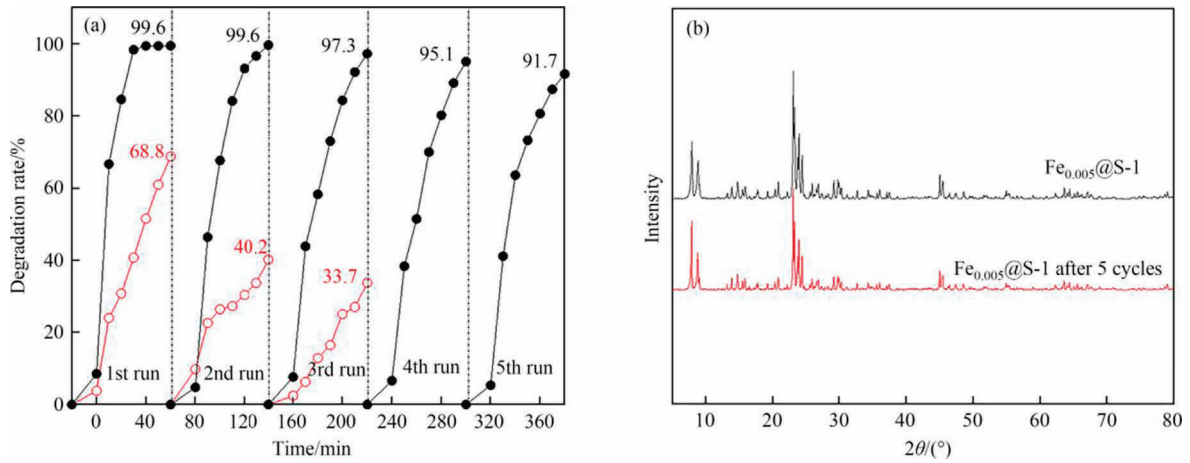

Fig. 9. (a) The recycling MB degradation performances of $Fe_{0.005}$@S-1 and Fe/S-1 catalysts (black symbol and line represent $Fe_{0.005}$@S-1, which red symbol and line represents Fe/S-1), and (b) XRD spectra of $Fe_{0.005}$@S-1 before and after five cycling tests. Reaction condition: [MB] = 10 mg·L^{-1}, catalyst = 0.5 g·L^{-1}, [H_2O_2] = 4 mmol·L^{-1}, T = 60 °C, initial solution pH = 2.

Table 1
Comparison of the degradation efficiency of MB over various Fe-based catalysts

Catalysts	Catalyst dose/mg·L^{-1}	Initial MB concentration/mg·L^{-1}	Temperature/°C	Initial pH value	Time/min	Degradation efficiency/%	Reference
Fe_3O_4/GO	2.92	5	60	3	60	97	[26]
Fe_3O_4@PDA-MnO_2	200	40	–	3	240	97	[27]
Fe_3O_4-MWCNTs	1000	40	60	3–5	70	94	[28]
Fe-NGLC	100	100	60	4	60	100	[29]
$FeCo_2O_4$-N-C	200	50	30	–	40	100	[30]
$CuFe_2O_4$	100	50	25	3.2	40	74	[31]
AC/γ-Fe_2O_3	2000	100	25	5	15	100	[32]
Fe@S-1	500	10	60	2	30	99	This work

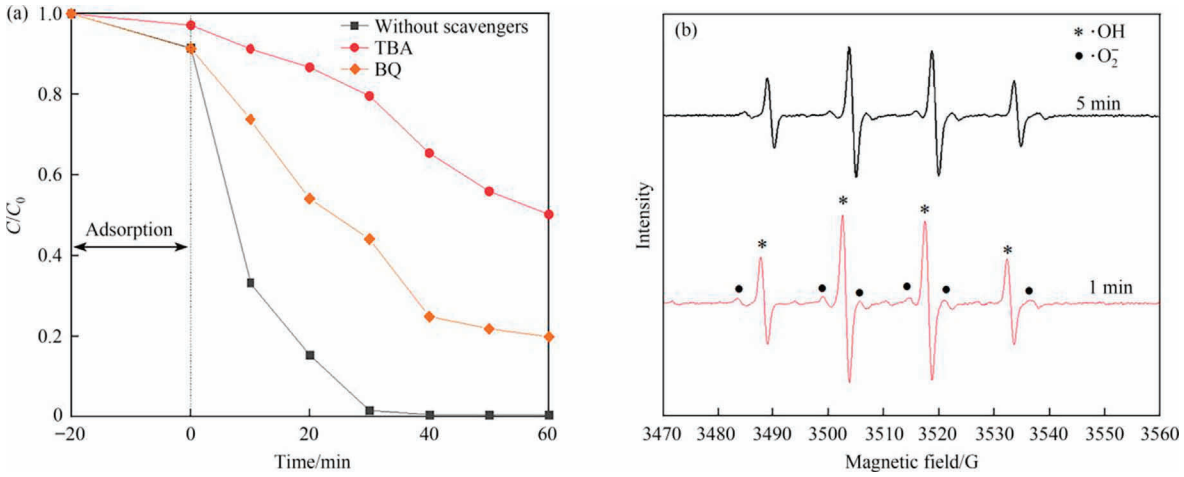

Fig. 10. (a) Catalytic degradation performances of MB over the $Fe_{0.005}$@S-1 catalyst with the addition of ·OH and $\cdot O_2^-$ scavenger, and (b) ESR measurements were carried out (·OH and $\cdot O_2^-$ were trapped by DMPO in aqueous solution). Experimental conditions: [MB] = 10 mg·L^{-1}, [catalyst] = 500 mg·L^{-1}, [H_2O_2] = 4 mmol·L^{-1}, [DMPO] = 100 mmol·L^{-1}.

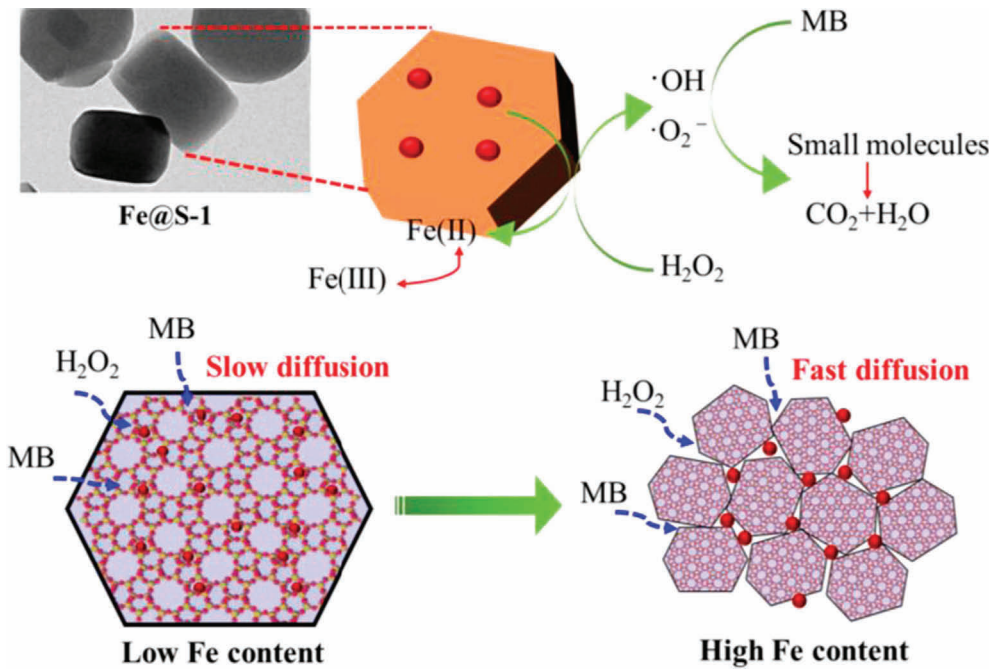

Fig. 11. Catalytic degradation mechanism of MB over the Fe@S-1 catalyst.

$$Fe(II) + H_2O_2 \rightarrow Fe(III) + \cdot OH + OH^- \quad (2)$$

$$Fe(II) + \cdot OH \rightarrow Fe(III) + OH^- \quad (3)$$

$$Fe(III) + H_2O_2 \rightarrow Fe(II) + \cdot O_2^- + 2H^+ \quad (4)$$

4. Conclusions

In heterogeneous Fenton-like degradation process, the leaching of Fe species is the main reason of the poor activity and stability of the catalysts as well as secondary pollution, which is considered a major challenge for practical application of wastewater treatment technology. Zeolite-encapsulated metallic catalysts as promising alternatives to the conventional impregnated catalysts show the potential for intensifying the advanced oxidation processes. In this work, Fe nanocatalysts are encapsulated within S-1 zeolite using a ligand-protected method with dicyandiamide as an organic ligand, then used for intensifying the catalytic degradation process of MB. Comparative HRTEM characterization of the zeolite encapsulated Fe nanocatalysts showed that the *in situ* encapsulation strategy can prepare highly-dispersed and ultrasmall Fe nanoparticles. Notably, the encapsulation strategy also enabled a relatively lower Fe loading in the Fe@S-1 catalyst in comparison with that of the impregnated Fe/S-1 catalyst, *i.e.*, 0.35% *vs.* 0.81 %(mass). The encapsulated Fe@S-1 catalyst demonstrated excellent catalytic activity and durability, outperformed the bulk Fe/S-1 catalyst prepared by impregnation method. Specifically, the Fe@S-1 catalyst showed high catalytic MB degradation efficiency of 100% in 30 min and good stability (only ~ 7.9% activity loss after five cycling tests). In addition, radical scavenging experiments and following ESR measurements indicated the major role of ·OH in the MB degradation process. The degradation mechanism of MB over the encapsulated Fe@S-1 catalyst was also proposed. During the catalytic

degradation process, the MB and H_2O_2 molecules diffused in the voids (which has large pore size of 1–2 nm) among the primary particles of the zeolite and interact with Fe(Ⅱ) species from Fe complexes/nanoclusters which were encapsulated in the Fe@S-1 with high molar ratio of [Fe(DCD)]Cl_3. However, when the molar ratio of [Fe(DCD)]Cl_3 is very low, the diffusion and accessibility of reactants and products to Fe active sites could be significantly limited due to that most of Fe species were atomically incorporated into the zeolite framework, and thus exhibiting a relatively lower degradation efficiency. The developed zeolite encapsulated Fe nanocatalysts can be further explored to overcome the challenging limitations normally encountered in Fenton-like degradation, *e.g.,* poor catalysts durability with high metal leaching, and thus being further explored for advanced catalytic oxidation process for practical wastewater treatment process.

Declaration of Competing Interest

The authors declare that they have no known competing financial interests or personal relationships that could have appeared to influence the work reported in this paper.

Acknowledgements

It is greatly appreciate the funding support from the Jiangsu Province Dual Creative Phds Program (JSSCBS20210400), and the Jiangsu Specially-Appointed Professors Program.

Supplementary Material

Supplementary data to this article can be found online at https://doi.org/10.1016/j.cjche.2022.03.010.

References

[1] R.Y. Dou, H. Cheng, J.F. Ma, Y. Qin, Y. Kong, S. Komarneni, Catalytic degradation of methylene blue through activation of bisulfite with CoO nanoparticles, *Sep. Purif. Technol.* 239 (2020) 116561.
[2] Y. Yin, L. Shi, W.L. Li, X.N. Li, H. Wu, Z.M. Ao, W.J. Tian, S.M. Liu, S.B. Wang, H.Q. Sun, Boosting Fenton-like reactions via single atom Fe catalysis, *Environ. Sci. Technol.* 53 (19) (2019) 11391–11400.
[3] X. Dong, Y.C. Lin, G.L. Ren, Y.Q. Ma, L. Zhao, Catalytic degradation of methylene blue by Fenton-like oxidation of Ce-doped MOF, *Colloids Surf. A Physicochem. Eng. Aspects* 608 (2021) 125578.
[4] C. Lai, F.L. Huang, G.M. Zeng, D.L. Huang, L. Qin, M. Cheng, C. Zhang, B.S. Li, H. Yi, S.Y. Liu, L. Li, L. Chen, Fabrication of novel magnetic $MnFe_2O_4$/bio-char composite and heterogeneous photo-Fenton degradation of tetracycline in near neutral pH, *Chemosphere* 224 (2019) 910–921.
[5] J.L. Wang, J.T. Tang, Fe-based Fenton-like catalysts for water treatment: catalytic mechanisms and applications, *J. Mol. Liq.* 332 (2021) 115755.
[6] C.Y. Dai, A.F. Zhang, L. Luo, X.B. Zhang, M. Liu, J.H. Wang, X.W. Guo, C.S. Song, Hollow zeolite-encapsulated Fe-Cu bimetallic catalysts for phenol degradation, *Catal. Today* 297 (2017) 335–343.
[7] J.R. Yang, D.Q. Zeng, Q.G. Zhang, R.F. Cui, M. Hassan, L.Q. Dong, J. Li, Y.L. He, Single Mn atom anchored on N-doped porous carbon as highly efficient Fenton-like catalyst for the degradation of organic contaminants, *Appl. Catal. B Environ.* 279 (2020) 119363.
[8] J.R. Yang, D.Q. Zeng, J. Li, L.Q. Dong, W.J. Ong, Y.L. He, A highly efficient Fenton-like catalyst based on isolated diatomic Fe-Co anchored on N-doped porous carbon, *Chem. Eng. J.* 404 (2021) 126376.
[9] X.H. Wang, Z.D. Nan, Highly efficient Fenton-like catalyst Fe-g-C_3N_4 porous nanosheets formation and catalytic mechanism, *Sep. Purif. Technol.* 233 (2020) 116023.
[10] P. Shukla, S.B. Wang, H.Q. Sun, H.M. Ang, M. Tadé, Adsorption and heterogeneous advanced oxidation of phenolic contaminants using Fe loaded mesoporous SBA-15 and H_2O_2, *Chem. Eng. J.* 164 (1) (2010) 255–260.
[11] X.F. Li, X. Liu, L.L. Xu, Y.Z. Wen, J.Q. Ma, Z.C. Wu, Highly dispersed Pd/PdO/Fe_2O_3 nanoparticles in SBA-15 for Fenton-like processes: confinement and synergistic effects, *Appl. Catal. B Environ.* 165 (2015) 79–86.
[12] Y.B. Wang, H.Y. Zhao, G.H. Zhao, Iron-copper bimetallic nanoparticles embedded within ordered mesoporous carbon as effective and stable heterogeneous Fenton catalyst for the degradation of organic contaminants, *Appl. Catal. B Environ.* 164 (2015) 396–406.
[13] N. Wang, Q.M. Sun, R.S. Bai, X. Li, G.Q. Guo, J.H. Yu, In situ confinement of ultrasmall Pd clusters within nanosized silicalite-1 zeolite for highly efficient catalysis of hydrogen generation, *J. Am. Chem. Soc.* 138 (24) (2016) 7484–7487.
[14] Q.M. Sun, N. Wang, Q.Y. Fan, L. Zeng, A. Mayoral, S. Miao, R.O. Yang, Z. Jiang, W. Zhou, J.C. Zhang, T.J. Zhang, J. Xu, P. Zhang, J. Cheng, D.C. Yang, R. Jia, L. Li, Q.H. Zhang, Y. Wang, O. Terasaki, J.H. Yu, Frontispiece: subnanometer bimetallic platinum–zinc clusters in zeolites for propane dehydrogenation, *Angewandte Chemie Int. Ed.* 59 (44) (2020) 19450–19459.
[15] Q.M. Sun, N. Wang, Q.M. Bing, R. Si, J.Y. Liu, R.S. Bai, P. Zhang, M.J. Jia, J.H. Yu, Subnanometric hybrid Pd-M$(OH)_2$, M = Ni, Co, clusters in zeolites as highly efficient nanocatalysts for hydrogen generation, *Chem.* 3 (3) (2017) 477–493.
[16] J. Zhu, R. Osuga, R. Ishikawa, N. Shibata, Y. Ikuhara, J.N. Kondo, M. Ogura, J.H. Yu, T. Wakihara, Z.D. Liu, T. Okubo, Ultrafast encapsulation of metal nanoclusters into MFI zeolite in the course of its crystallization: catalytic application for propane dehydrogenation, *Angewandte Chemie Int. Ed.* 59 (44) (2020) 19669–19674.
[17] Q.M. Sun, N. Wang, T.J. Zhang, R.S. Bai, A. Mayoral, P. Zhang, Q.H. Zhang, O. Terasaki, J.H. Yu, Zeolite-encaged single-atom rhodium catalysts: highly-efficient hydrogen generation and shape-selective tandem hydrogenation of nitroarenes, *Angew. Chem. Int. Ed Engl.* 58 (51) (2019) 18570–18576.
[18] H.J. Cho, D. Kim, J. Li, D. Su, B.J. Xu, Zeolite-encapsulated Pt nanoparticles for tandem catalysis, *J. Am. Chem. Soc.* 140 (41) (2018) 13514–13520.
[19] N. Wang, Q.M. Sun, J.H. Yu, Ultrasmall metal nanoparticles confined within crystalline nanoporous materials: a fascinating class of nanocatalysts, *Adv. Mater.* 31 (1) (2019) 1803966.
[20] Z.Y. Jiang, L.Z. Wang, J.Y. Lei, Y.D. Liu, J.L. Zhang, Photo-Fenton degradation of phenol by CdS/rGO/Fe^{2+} at natural pH with in situ-generated H_2O_2, *Appl. Catal. B Environ.* 241 (2019) 367–374.
[21] D. Chlebda, P. Stachurska, R. Jędrzejczyk, Ł. Kuterasiński, A. Dziedzicka, S. Górecka, L. Chmielarz, J. Łojewska, M. Sitarz, P. Jodłowski, DeNO_x abatement over sonically prepared iron-substituted Y, USY and MFI zeolite catalysts in lean exhaust gas conditions, *Nanomaterials* 8 (1) (2018) 21.
[22] A. Hussain, D.W. Sun, H.B. Pu, Bimetallic core shelled nanoparticles (Au@AgNPs) for rapid detection of thiram and dicyandiamide contaminants in liquid milk using SERS, *Food Chem.* 317 (2020) 126429.
[23] K. Bian, A.F. Zhang, H. Yang, B.H. Fan, S.T. Xu, X.W. Guo, C.S. Song, Synthesis and characterization of Fe-substituted ZSM-5 zeolite and its catalytic performance for alkylation of benzene with dilute ethylene, *Ind. Eng. Chem. Res.* 59 (52) (2020) 22413–22421.
[24] J.Y. Wang, G.N. Li, X.H. Ju, H.A. Xia, F.T. Fan, J.H. Wang, Z.C. Feng, C. Li, Identification of $Fe_2(\mu\text{-}O)$ and $Fe_2(\mu\text{-}O)_2$ sites in Fe/ZSM-35 by in situ resonance Raman spectroscopy, *J. Catal.* 301 (2013) 77–82.
[25] S.L. Deng, X.B. Zhang, G.J. Lv, Y. Zhai, Z.B. Yang, Y.Q. Zhu, H.C. Li, F.M. Wang, Influence of zeolite carriers on the dyes degradation for framework Fe-doped zeolite catalysts, *J. Sol Gel Sci. Technol.* 91 (1) (2019) 54–62.
[26] S.J. Song, Y.L. Wang, H. Shen, J. Zhang, H. Mo, J. Xie, N.L. Zhou, J. Shen, Ultrasmall graphene oxide modified with Fe_3O_4 nanoparticles as a Fenton-like agent for methylene blue degradation, *ACS Appl. Nano Mater.* 2 (11) (2019) 7074–7084.
[27] X.H. Pan, S.Y. Cheng, T. Su, G.C. Zuo, W. Zhao, X.L. Qi, W. Wei, W. Dong, Fenton-like catalyst Fe_3O_4@polydopamine-MnO_2 for enhancing removal of methylene blue in wastewater, *Colloids Surf. B Biointerfaces* 181 (2019) 226–233.
[28] A. Tolba, M. Gar Alalm, M. Elsamadony, A. Mostafa, H. Afify, D.D. Dionysiou, Modeling and optimization of heterogeneous Fenton-like and photo-Fenton processes using reusable Fe_3O_4-MWCNTs, *Process. Saf. Environ. Prot.* 128 (2019) 273–283.
[29] B. Ren, J.F. Miao, S.S. Wang, Y.L. Xu, Z.Z. Zhai, X.X. Dong, Z.F. Liu, Facilely synthesized porous 3D coral-like Fe-based N-doped carbon composite as effective Fenton catalyst in methylene blue degradation, *Colloids Surf. A Physicochem. Eng. Aspects* 618 (2021) 126439.
[30] T. Zhang, Q.Q. Ma, M.Q. Zhou, C.Y. Li, J.C. Sun, W.J. Shi, S.Y. Ai, Degradation of methylene blue by a heterogeneous Fenton reaction catalyzed by $FeCo_2O_4$-N-C nanocomposites derived by ZIFs, *Powder Technol.* 383 (2021) 212–219.
[31] Q.D. Qin, Y.H. Liu, X.C. Li, T. Sun, Y. Xu, Enhanced heterogeneous Fenton-like degradation of methylene blue by reduced $CuFe_2O_4$, *RSC Adv.* 8 (2) (2018) 1071–1077.
[32] M. Fayazi, M.A. Taher, D. Afzali, A. Mostafavi, Enhanced Fenton-like degradation of methylene blue by magnetically activated carbon/hydrogen peroxide with hydroxylamine as Fenton enhancer, *J. Mol. Liq.* 216 (2016) 781–787.